Self-healable Waterborne Poly(urethane/acrylic) Hybrid Dispersion

Highlights

This chapter discloses an easy but productive strategy that is based on the triple synergistic effect of 'dynamic hard domain', 'multiple hierarchical hydrogen bonding', and 'semi-interpenetrating network (IPN) formation', to address the eternal dilemma existed between high healing efficiency and mechanical robustness. The dynamic disulfide bond of 2-aminophenyl disulfide (2-APDS) and multiple hierarchical hydrogen bonding raised from urea and urethane linkages supplement the healing ability, concurrently, polyacrylates and rigid aromatic moiety improve the mechanical properties of self-healing poly(urethane-acrylic) (SWPUA) films. Owing to the judicious molecular engineering and aforementioned tactic, a series of SWPUA films were prepared by using 2-APDS as the 'dynamic hard domain', monoglyceride of castor oil (MG_{CO}) as a chain extender, glycerol ester of citric acid (GECA) as an internal emulsifier and different acrylate monomers with other desired reactants (polyols/diamines and diisocyanate). The resulting films exhibited good mechanical robustness, high thermal stability, and biodegradability. Notably, the maximum healing efficiency of 82.53% was achieved within 330 s under microwave exposure (800 W) and the cut films were re-processable at 60 °C under a pressure of 60-80 $kgcm^{-2}$. Most importantly, the MTT (3-[4,5-dimethylthiazol-2-yl]-2,5 diphenyl tetrazolium bromide) and live/dead assays of mouse fibroblast cell lines (L929) treated with a representative SWPUA dispersion (up to 30%) confirmed its biocompatibility. Most interestingly, SWPUA can be employed to prepare SWPUA/GelMA (gelatin methacryloyl)/gelatin hybrid ink for the development of 3D printable biomedical scaffolds.

Parts of this chapter are published in

Morang, S., Rajput, J. H., Mukherjee, A., Poundarik, A., Das, B. and Karak, N. A dynamic hard domain induced self-healable waterborne poly (urethane/acrylic) hybrid dispersion for 3D printable biomedical scaffolds. *Materials Advances*, 4:4784-4797, 2023. (DOI: 10.1039/D3MA00607G)

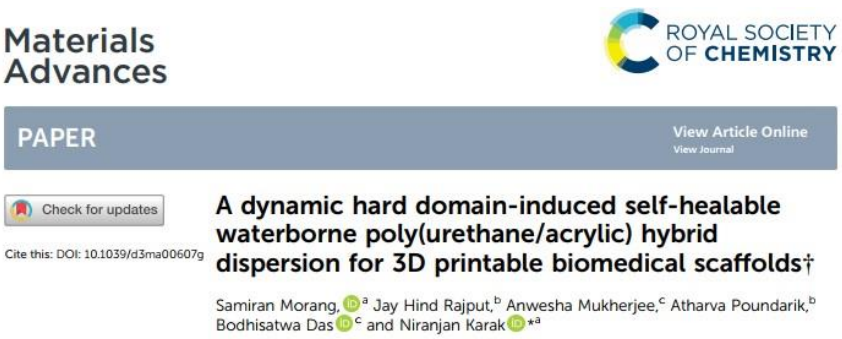
Materials Advances

ROYAL SOCIETY OF CHEMISTRY

PAPER

View Article Online
View Journal

Check for updates

Cite this: DOI: 10.1039/d3ma00607g

A dynamic hard domain-induced self-healable waterborne poly(urethane/acrylic) hybrid dispersion for 3D printable biomedical scaffolds†

Samiran Morang,[a] Jay Hind Rajput,[b] Anwesha Mukherjee,[c] Atharva Poundarik,[b] Bodhisatwa Das[c] and Niranjan Karak[*a]

3.1. Introduction

As discussed in **Chapter 1** and **Chapter 2**, waterborne polyurethane (WPU) is one of the sought-after polymers because of its environmentally friendly character and magnificent performance [1]. But like other polymers, WPUs are also susceptible to damage in byzantine and harsh environments throughout their lifecycle. Premature damage crops up due to the presence of small imperfections or micro-cracks of the materials. Some of these cracks are inherent and arduous to repair. This results in catastrophic failure of the materials before their desired service life. Nowadays, researchers mimic the renowned natural phenomena of self-healing to resolve these problems [2]. All living organisms can mend minor or major damages by themselves without any external stimuli, which contribute to their longevity. The introduction of self-healing features into WPU is a very enthusiastic field of research. This salient feature greatly enhances the reliability and longevity of WPU. Furthermore, it improves safety in service, decreases raw material consumption, reduces carbon emissions, and above all minimizes maintenance costs. Thus, the ultimate self-healing WPU (SWPU) become a promising futuristic material having numerous potential applications in the field of smart coatings, wearable and flexible electronics, and sensors, along with others. Notably, the favorable conditions (high chain mobility, and exchange of dynamic bonds) for self-healing always conflict with the indispensable conditions (high chain rigidity, intermolecular interaction, and crystallinity) for mechanical strength. So, the efficient self-healing and high mechanical strength of WPUs are two contradictory properties. Thus, simultaneous improvement of these two vital properties is always a formidable challenge. Previously, several scientists have proposed ingenious strategies to address this issue. However, the most used strategies include the introduction of an asymmetric alicyclic structure adjacent to an aromatic disulfide molecule [3], dynamic hard domain [4], synergistic triple dynamic bonds [5], etc.

In this regard and concerning environment benign-ness, a series of organic solvent-free, and surfactant-free self-healable WPU/polyacrylic (SWPUA) dispersions were synthesized using 2-APDS as the 'dynamic hard domain' along with other required reactants and different acrylate monomers. Here, acrylate monomers were used as the diluent to the polymerization medium at the beginning and polymerized via the seeded mini-emulsion polymerization technique at the final stage to obtain the desired dispersion. Remarkably, the resultant dispersion is highly stable for up to six months (zeta potential -47.1 mV to -60.4 mV) and all SWPUA films exhibited good healing efficiency, mechanical robustness, thermal re-processability, and biodegradability. Most importantly, the MTT (3-[4,5-dimethylthiazol-2-yl]-2,5 diphenyl tetrazolium bromide) assay and live/dead assay of mouse fibroblast cell

lines (L929) treated with a representative SWPUA (SWPUA-2) dispersion confirm biocompatibility. Furthermore, we have explored the 3D printability nature of SWPUA-2 dispersion by preparing SWPUA-2/ gelatin methacryloyl (GelMA)/gelatin hybrid ink which was used for the development of 3D-printable biomedical scaffold.

3.2. Experimental

3.2.1. Materials

Reactants such as isophorone diisocyanate (IPDI), poly(ε-caprolactone diol) ε-PCL_{2000}, dimethyl hydroxy propionic acid (DMPA), citric acid, glycerol, castor oil, triethyl amine (TEA), *para*-toluene sulphonic acid (*p*-TSA), and CaO have the same specification and grade as mentioned in **Chapter 2**, **Section 2.2.1**.

bis(2-Aminophenyl) disulfide (2-APDS, Sigma Aldrich; 97%) is used as the dynamic hard domains and chain extender. It is a yellowish-amber green color crystalline solid with molecular weight and the melting point of 248.37 $gmol^{-1}$ and 91-92 ℃, respectively.

1,6-Diaminohexane (HMDA, Sigma Aldrich; 98%) is also used as the chain extender, having a molecular weight of 116.20 $gmol^{-1}$, density of 0.84 gmL^{-1}, and a melting point of 42 ℃.

Potassium persulfate (KPS, Sigma Aldrich; ≥99%) is an odorless white powder with a molecular weight of 270.322 $gmol^{-1}$ and it was used as the initiator in the free-radical polymerization.

Dibutyltin dilaurate (DBTDL, Sigma Aldrich; 95%) is a colorless viscous, and oily liquid, used as catalyst in PU reactions. It has a molecular weight, density, and a melting point of 631.56 $gmol^{-1}$, 1.066 gmL^{-1}, and 22-24 ℃, respectively.

Methyl methacrylate (MMA, Sigma Aldrich; 99%) is a colorless liquid with a molecular weight of 100.12 $gmol^{-1}$, density of 0.94 gmL^{-1}, and a boiling point of 101 ℃. It was used as an acrylate monomer.

Butyl acrylate (BA, Sigma Aldrich; ≥99%) was employed as acrylate monomer and it has a molecular weight, density, and a boiling point of 128.17 $gmol^{-1}$, 0.89 gmL^{-1}, and 148 ℃, respectively.

2-Hydroxyethyl methacrylate (HEMA, Sigma Aldrich; ≥99%) is a colorless viscous liquid with a molecular weight of 130.143 $gmol^{-1}$, density of 1.07 gmL^{-1}, and a boiling point of 250 ℃. It was used as a monomer to prepare polyacrylic.

Glycidyl methacrylate (GMA, Sigma Aldrich; ≥97%) is a clear, colorless liquid with a strong ester and fruity odor. It has a molecular weight, density, and a boiling point of 142.15 $gmol^{-1}$, 1.07 gmL^{-1}, and 189 °C, respectively. It was also used as an acrylate monomer.

3.2.2. Methods

3.2.2.1. Preparation of monoglyceride of castor oil (MG_{CO})

MG_{CO} was prepared by glycerolysis of castor oil using the same chemicals and conditions as mentioned in **Chapter 2**, **section 2.2.2.1**.

3.2.2.2. Preparation of glycerol ester of citric acid (GECA)

GECA was prepared by the esterification reaction of citric acid and glycerol using the same conditions as reported in **Chapter 2**, **section 2.2.2.2**.

Table 3.1. Recipes for the synthesis of SWPUAs with constant disulfide content (4.5 wt%).

Reactant/ Composition	SWPUA-1	SWPUA-2	SWPUA-3	SWPUA-4
ϵ-PCL (mM)	1	1	1	1
DMPA (mM)	1.5	1.5	1.5	1.5
GECA (mM)	0.375	0.375	0.375	0.375
MG_{CO}(mM)	1	1	1	1
2-APDS (mM)	0.80	0.80	0.80	0.80
HMDA (mM)	0.35	0.35	0.35	0.35
IPDI (mM)	6.65	6.65	6.65	6.65
TEA (mM)	1.575	1.575	1.575	1.575
MMA (mM)	44.145	35.316	35.316	22.073
2-HEA (mM)	0	6.792	0	0
GMA (mM)	0	0	6.218	0
BA (mM)	0	0	0	17.241

3.2.2.3. Preparation of SWPUA dispersions

The reaction setup for preparing SWPUA dispersions consists of a 100 mL three-neck round bottom flask equipped with a nitrogen inlet, a thermometer, a septum, and a Teflon blade

stirrer. The formulations of various PU-acrylates (PUAs) are presented in **Table 3.1.** For the synthesis of the NCO-terminated prepolymer, ε-PCL_{2000} (1 mM), DMPA (1.5 mM), IPDI (3 mM), DBTDL (0.05 wt% of PU), and 25% of acrylate monomers were added into the round bottom flask. The prepolymer formation was confirmed by FTIR spectral analysis. Then, 2-APDS (0.80 mM), GECA (0.375 mM), MG_{CO} (1 mM), 25% acrylate monomers, and remaining IPDI (3.65 mM) were added to the mixture and continued for 3-4 h at 70 ℃. Then, the reaction mixture was cooled to 25-30 ℃, and TEA (2.81 mM) and the remaining 50% of acrylate monomers were added to the mixture and stirred for 45 min under the same conditions to neutralize the carboxylic groups of GECA and DMPA. Subsequently, the aqueous dispersion was prepared by adding double de-ionized water to the prepolymer-monomer mixture at the same temperature within 15 min under high agitation (750 rpm). Then, HMDA (0.35 mM) was added, and the reaction was continued for 1 h at 70 ℃. Finally, acrylate monomers were polymerized via a free radical chain-growth polymerization mechanism. The reaction was performed for 2 h at 70 ℃ by adding KPS solution in water (1 g) in a single shot. Finally, a stable whitish SWPUA dispersion was obtained.

3.2.2.4. Preparation of SWPUA films

The synthesized SWPUA dispersions were cast on different flat surfaces for different tests and analyses. The films cast on metal steel plates (150 mm × 50 mm × 5 mm) were used for the impact resistance study, on glass slides (80 mm × 30 mm × 10 mm) were used for scratch hardness tests, and on Teflon sheets, the films were used for tensile strength, elongation, toughness, etc. measurements. All the films were dried at room temperature for 2 days followed by vacuum drying at an elevated temperature to remove the remaining solvent and kept in a desiccator. All the films were kept under ambient conditions for 2 days before their testing and analyses.

3.2.3 Characterization and tests

3.2.3.1. Structural characterization and property evaluation

SWPUA films were characterized by using various techniques as reported in **Chapter 2** or other techniques as listed follows. The ^{1}H and ^{13}C NMR spectra of SWPUA-2 were recorded by a Bruker Biospin AG 500 MHz NMR spectrometer (Model- Avance III HDX, USA) using DMSO-d_6 as the solvent and TMS as the reference. Similarly, physico-chemical and thermo-mechanical properties were evaluated using different tests as mentioned in **Chapter 2**. Additionally, the average particle size of the SWPUA dispersions was measured by a NanoPlus dynamic light scattering (DLS, Particulate System, USA) and investigated further

by high resolution transmission electron microscope (HR-TEM, 300 kV, Tecnai G2, F30, FEI, USA).

3.2.3.2. Self-healing (SH) test

The SH ability of the SWPUAs has been evaluated both quantitatively and qualitatively. To investigate the healing performance, the rectangular specimens of ~ 40 mm × 10 mm × 0.55 mm (length × width × thickness) were cut in a transverse direction (length ~ 5 mm) by a sharp razor blade. The damaged area was healed using a domestic microwave oven at different powers (600 W, 700 W, and 800 W). The healed and unhealed areas were tracked using an optical microscope. Weightlifting and stretching tests were also performed after healing. In this study, the healing efficiency was defined as the ratio of restored tensile strength after healing to the original tensile strength and calculated according to **Eq. 3.1**. At least three healed specimens of each sample were analyzed by measuring the tensile strength.

$$\text{Self} - \text{healing efficiecny}, \eta_h(\%) = \frac{\sigma_h}{\sigma_o} \times 100 \qquad \textbf{Eq. 3. 1}$$

Here, σ_o is the tensile strength of the pristine film, and σ_h is the tensile strength of the healed film.

3.2.3.3. Re-processability test

To investigate the reprocessing performance, the films were cut into small pieces with the dimension of ~ 2.5 mm × 2.5 mm × 0.55 mm (length × width × thickness). The pieces were reprocessed by hot-pressing. The change in the tensile strength was evaluated after the physical reprocessing. The recycling efficiency is calculated according to **Eq. 3.2**.

$$\text{Reprocessing efficiecny}, \eta_r(\%) = \frac{\sigma_r}{\sigma_o} \times 100 \qquad \textbf{Eq. 3. 2}$$

Here, σ_o is the tensile strength of the original film, and σ_r is the tensile strength of the reprocessed film.

3.2.3.4. Cell culture and maintenance

The cytotoxicity and cytocompatibility of SWPUA-2 polymer were studied against mouse fibroblast cell lines (L929), as these cells are responsible for extracellular matrix production. Cells were maintained and cultivated following the standard protocol. Briefly, cells were grown in a sterile incubator at 37 ℃with 5% CO_2 and >90% humidity. After that, cells were taken out and allowed to reach 80–90% confluence in the high glucose DMEM growth medium (Gibco, USA) containing 10% fetal bovine serum (FBS, Gibco, USA) and 1%

antibiotic-antimycotic solution (Himedia, India). After removing the medium, sterile PBS was used to wash the cells. The cells were then trypsinized and moved to a new flask with a fresh growth medium.

3.2.3.5. *In Vitro* cytotoxicity evaluation

3.2.3.5.1. Cell proliferation analysis by MTT assay

In vitro cytocompatibility assay was carried out using L929 via cell viability [MTT] assay for a period of 3 days. Different concentrations of SWPUA-2 solutions (10%, 20%, and 30%) were sterilized for 1 h under exposure to UV radiation. The control sample was prepared without SWPUA-2. Then 100 µL of a cell suspension of 10^5 cellsmL^{-1} with DMEM complete medium was dispensed into the peripheral wells of a 96-well tissue culture microliter plate. After 24 h and 72 h of incubation medium was removed and replaced by fresh medium. Then MTT solution was added to the samples along with the control and incubated for 3 h. Then DMSO was added to each well and mixed well to solubilize the formazan crystal. The relative reduction in cell viabilities in comparison to the untreated control group was then measured at 570 nm using **Eq. 3.3**. Experiments were repeated three times.

$$\text{Cell viability (\%)} = \frac{\text{Mean optical density}}{\text{Control optical density}} \times 100 \qquad \textbf{Eq. 3.3}$$

3.2.3.5.2. Live/dead assay

Using live/dead assay following the manufacturer's instructions, cell viability was assessed after 3 days of seeding. Then different concentrations of SWPUA-2 samples were washed with PBS and incubated with calcein AM (4 mM, Merck, Germany) for staining live cells and ethidium bromide for staining dead cells (2 mM, Himedia, India) with serum-free DMEM for 45 min at 37 ℃ in a humidified incubator. Post-staining samples and control were washed with PBS and cells were imaged using a Leica fluorescence microscope (E_x = 501 nm; E_m = 521 nm and E_x = 301 nm; E_m = 603 nm for calcein AM and ethidium bromide). Experiments were performed thrice.

3.2.3.6. Preparation of SWPUA-2/GelMA (gelatin methacryloyl)/gelatin-based scaffolds using 3D bio-printer

By combining gelatin with GelMA (gelatin methacryloyl) following a well-studied method, and SWPUA-2 at appropriate concentrations was mixed, and ink was prepared. After that scaffolds were fabricated for biomedical applications. The GelMA was synthesized by adopting a synthesis method [6]; 0.5% (wt/v) Irgacure 2959 (photo-crosslinker) solution was prepared in Dulbecco's phosphate buffered saline (DPBS) [7] and added 20% wt/v

GelMA to obtain the final solution. An ANGA PRO 3D with a twin extruder bio-printer (ALFATEK SYSTEMS) was used to print the ink {(GelMA/ SWPUA-2)/Gelatin}. To get good mechanical stability, a photo crosslinker (Irgacure 2959) was used, which crosslinked to GelMA.

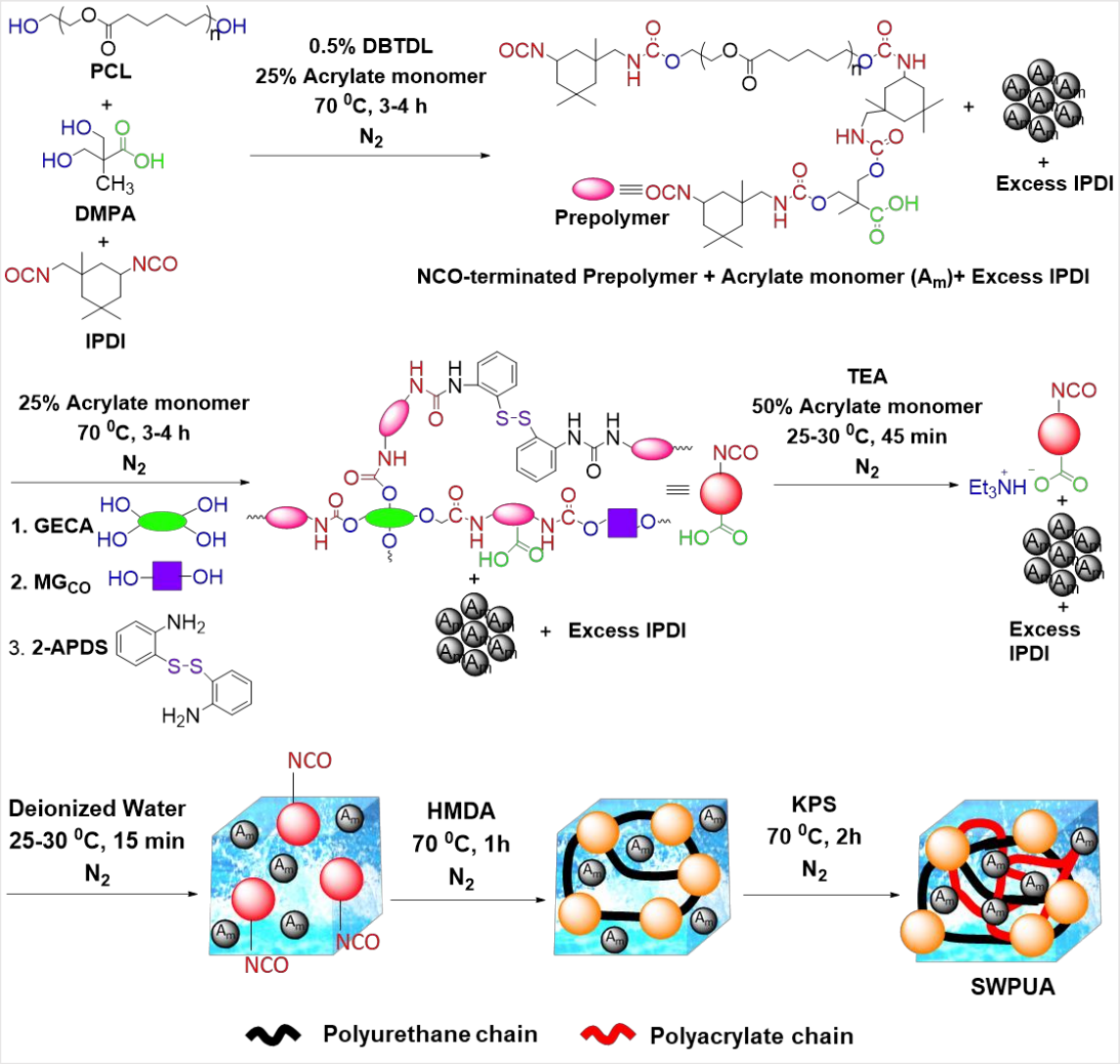

Scheme 3.1. The representative synthetic route for the synthesis of SWPUA dispersions.

The prepared solution of gelatin (20% wt/v) was added into the ink to help in printability and compensated for compromised printability by adding GelMA. The luer syringe attached with a 22 G conical tapered tip was utilized for making distinct scaffolds. The ink solution was kept for a few minutes at ambient temperature until the ink could show the printability having partially solidified and viscous characteristics. The cuboid design (2.5 cm × 2.5 cm × 1 cm) was created using the SOLIDWORKS 2021 student version design software in a.amf format. The .amf file was sliced and converted into the G.Code format with optimized process parameters using Cura_14.09 software. The G.Code file was loaded on Melzi-Mendel software, and then run to construct the scaffold on a petri dish.

3.2.3.7. Biodegradation test

The biodegradation of SWPUA was studied through a soil burial method. A calculated amount of each sample was put into a disposable teacup and buried inside soil 20-30 cm deep in an open area with Latitude- 26°41′56.7708″ and Longitude-92°50′2.8896″ for 120 days. The weight loss was calculated and the changes in the surface morphology of each sample were evaluated using a scanning electron microscope (SEM, Model-JSM 6390LV, Jeol, Japan).

3.3. Results and discussion

3.3.1. Synthesis and characterization of SWPUA dispersions and films

It is familiar that the healing efficiency is always associated with good chain mobility which opposes the high mechanical strength. To create a win-to-win situation, the rigidly structured 2-APDS and different acrylates were incorporated into the WPU system via a seed mini-emulsion polymerization. As shown in **Scheme 3.1**, a series of SWPUA hybrid dispersions with different acrylates (**Table 3.1**) were synthesized in the absence of solvent by step-growth and free radical chain-growth polymerization techniques, simultaneously. Here, HMDA is more nucleophilic than 2-HEMA towards NCO groups of IPDI. The chemical structure of the SWPUAs was confirmed by FTIR and NMR spectral analyses as discussed below. **Figure 3.1 (a)** and **(b)** shows the absorption peaks of various functional groups present in the synthesized polymer dispersions and prepolymer (SWPUA-2).

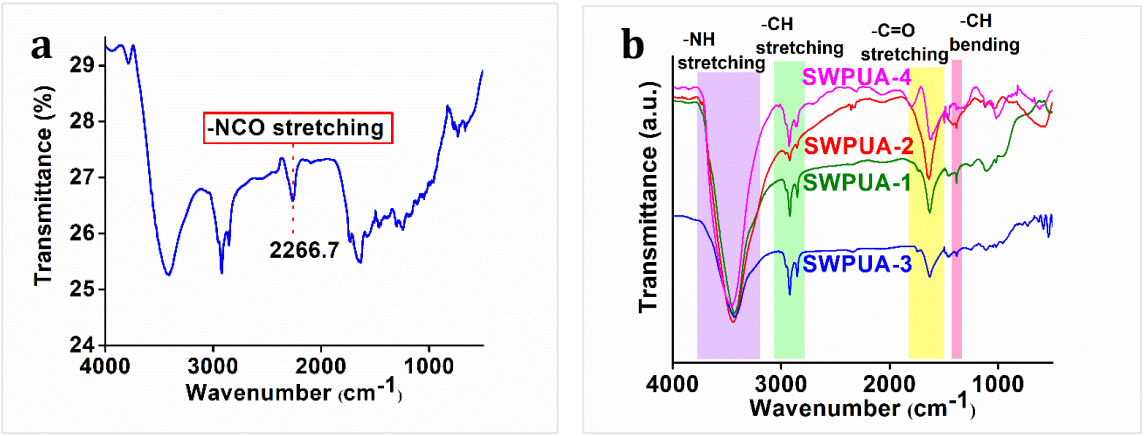

Figure 3.1. (a) FTIR spectrum of the prepolymer of SWPUA-2 and (b) FTIR spectra SWPUAs.

Notably, the characteristic absorption peaks –NCO and –OH groups were absent near 2267 cm^{-1} and 3500 cm^{-1}, respectively which confirmed that the –NCO group must be converted to either urethane or urea unit. A single peak of the –NH group was observed near 3400 cm^{-1}. The characteristic peaks at 2850 cm^{-1} and 2928 cm^{-1} can be assigned to the symmetric and asymmetric stretching vibrations of the –CH bond, respectively. The stretching vibration of the C=O group was observed at 1641 cm^{-1}. The peaks at 1106 cm^{-1} and

1244 cm^{-1} can be assigned to symmetric and asymmetric stretching vibrations of the C-O-C group. Further, the small band near 1461 cm^{-1} corresponds to the N–H bending vibration.

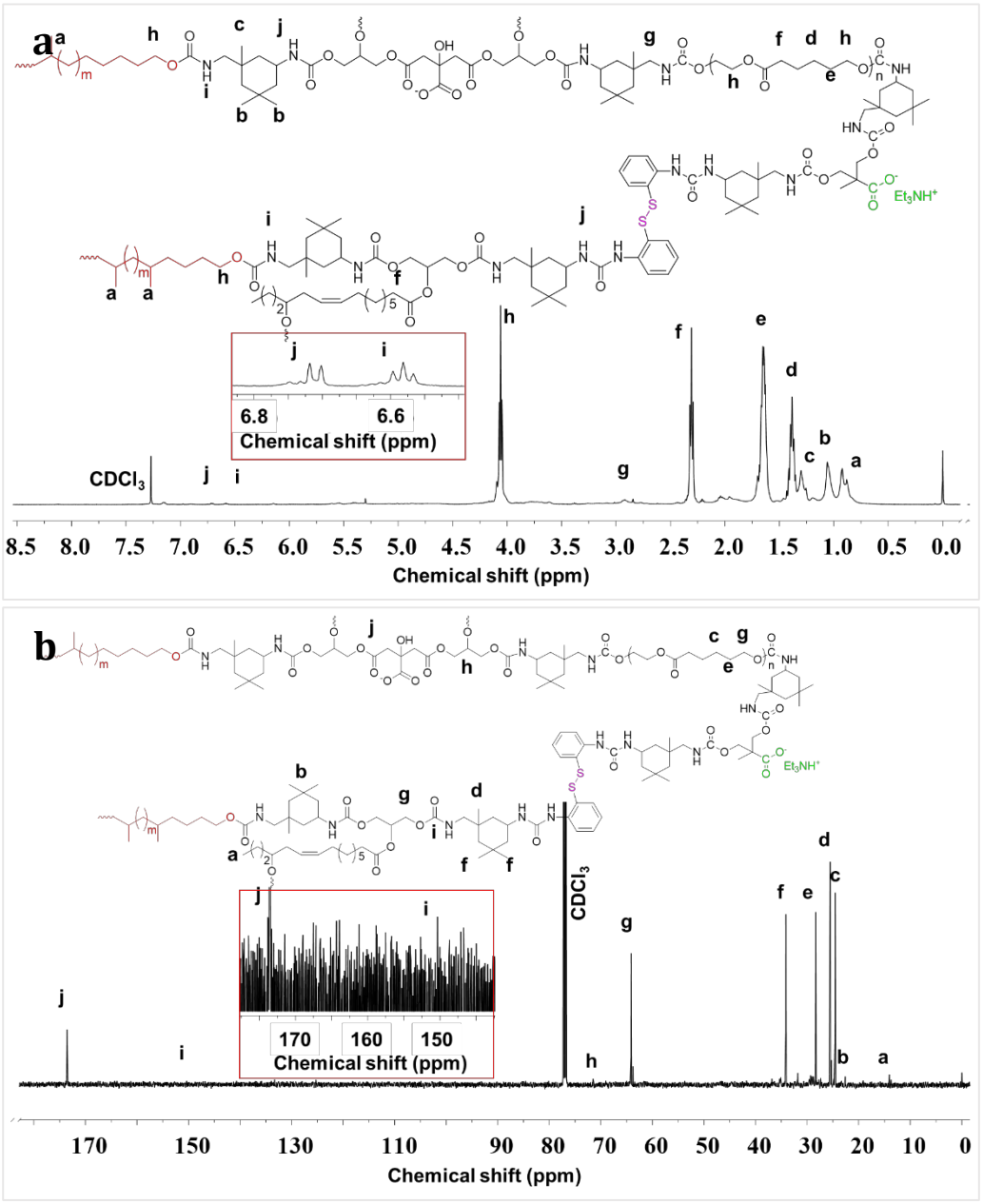

Figure 3.2. (a) 1H NMR spectrum and (b) 13C NMR spectrum of SWPUA-2.

These results suggested that urethane linkage had been formed. Finally, the proposed structure of the SWPUA-2 was confirmed by ^{1}H and ^{13}C NMR spectral analyses. The ^{1}H NMR spectrum of SWPUA-2 is shown in **Figure 3.2 (a)**. In the ^{1}H spectrum, the three peaks at 0.88 ppm (a), 1.06 ppm (b), and 1.30 ppm (c) correspond to the methyl protons present in the acrylates and IPDI moieties of the PU. The peaks at 1.38 ppm (d) and 1.65 ppm (e) correspond to the γ and β methylene protons of PCL units, respectively. The α-methylene proton of the ester linkage can be found at 2.31 ppm (f). The peaks at 2.92 ppm (g) and 4.05 ppm (h) can be assigned to the α-methylene proton present next to the N-atom and O-atom

of the carbamate group, respectively. Again, the proton attached to the N-atom of the primary and secondary isocyanates group was observed at 6.58 ppm (i) and 6.72 ppm (j), respectively [3]. Thus, the data of the ^{1}H NMR spectrum support the probable chemical structure of SWPUA-2 [5]. The structure was further confirmed by the ^{13}C NMR spectral analysis.

Table 3.2. Physical properties of SWPUAs and their films.

Sample	Appearance	Z-average size (nm)	Zeta potential (mV)	Molecular weight		PDI	Contact angle
				M_w ($gmol^{-1}$)	M_n ($gmol^{-1}$)		
SWPUA-1	Milky white	105.1	-50.6	173265	106876	1.621	84.7°
SWPUA-2	Milky white	135	-47.1	146783	91281	1.607	94.4°
SWPUA-3	Milky white	109.6	-50.0	151605	91996	1.647	86.1°
SWPUA-4	Milky white	115	-60.4	150189	92194	1.629	86.5°

The ^{13}C NMR spectrum of SWPUA-2 is shown in **Figure 3.2 (b)**. The peaks at 14 ppm (a) can be assigned to the terminal methyl carbon present in the MG_{CO} unit of the SWPUA-2. Again, the two types of methyl carbon available in IPDI moiety appeared at 25.43 ppm (d) and 34.12 ppm (f). The α, β, and γ-methylene carbon concerning the carbamate group were observed at 22.50 ppm (c), 28.34 ppm (e), and 64.01 ppm (g), respectively. A small peak at 71.53 ppm (h) can be assigned to the mid-carbon of the glycerol moiety. Furthermore, the carbonyl carbon present in the carbamate group and the ester groups were found at 150.36 ppm (i) and 173.36 ppm (j), respectively. Thus, all the peaks support the expected structure of the newly synthesized SWPUA-2.

3.3.2. Physical properties of SWPUA dispersions and films

The solubility test reveals that all SWPUA films are soluble in polar solvents such as THF, DMF, and DMSO but insoluble in non-polar solvents like hexane, toluene, and xylene. The synthesized polymer contains different polar functional groups such as carbamate group, ester group, and carboxylic acid on its surface which help the polymer chain to disperse in polar solvents. The physical properties of SWPUA dispersion and films were tabulated in **Table 3.2**. Results show that the particle sizes of SWPUA-1, SWPUA-2, SWPUA-3, and SWPUA-4 were 105.1 nm, 135 nm, 109.6 nm, and 115 nm, respectively. The digital images of

all SWPUAs, the TEM image of SWPUA-2, and the particle size distribution curves are shown in **Figure 3.3**. Importantly, the particle size of the dispersion is related to the weight percentage of the emulsifier and cross-linker (functionality, f ≥ 3) used [8].

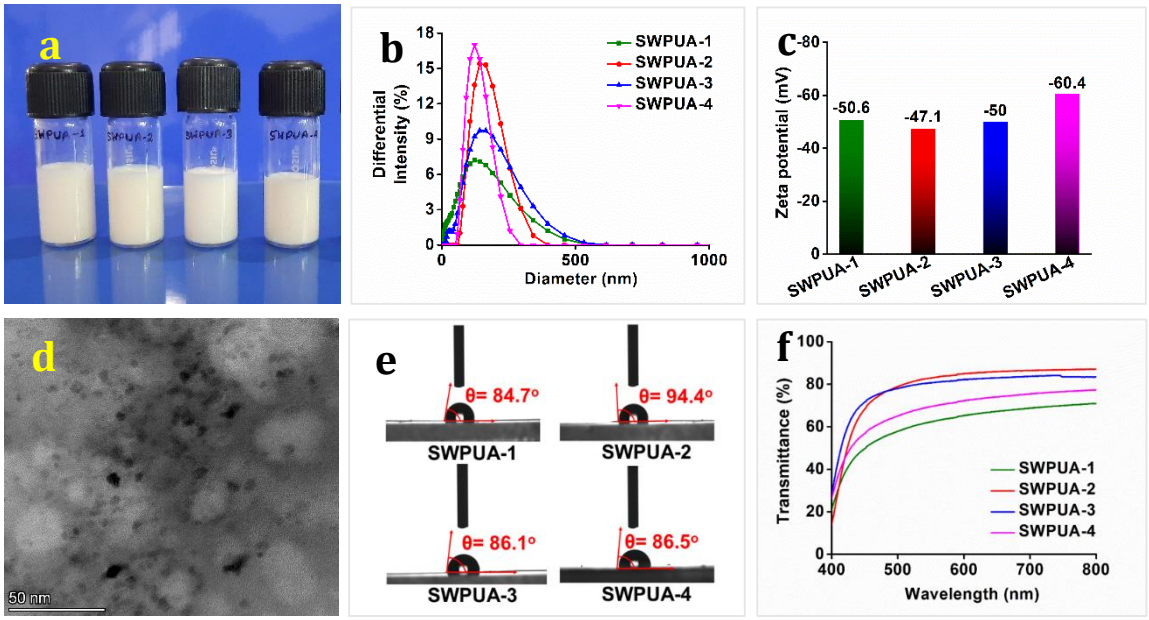

Figure 3.3. (a) Digital photos of SWPUA dispersions, (b) particle size distribution, (c) zeta potential (mV) of SWPUA dispersions, (d) TEM image of SWPUA-2 dispersion, (e) contact angle, and (f) percentage of transmittance of SWPUA films.

Higher content of cross-linker results in large particle size because of a high degree of branch formation. However, a higher amount of emulsifier produces a high surface charge density in the polymeric chain, generating electrostatic repulsion. This repulsion does not allow the polymeric particle to aggregate, resulting in a small particle size distribution. As all composition contains the same amount of DMPA (act as an internal emulsifier) and GECA (act as a bio-based internal emulsifier and cross-linker), the respective particle sizes are not very much deviated from each other. However, it can be seen clearly that SWPUA-2 possesses small particles as compared to other compositions, which can be attributed to the proper grafting of 2-HEMA to the PU backbone via the urethane linkage [9]. Thus, the narrow particle size distribution **Figure 3.3 (b)**, zeta potential (lower than -47 mV) (**Figure 3.3 (c)**), and TEM image (**Figure 3.3 (d)**), support the high stability of the resultant SWPUA dispersions. Again, **Figure 3.3 (e)** shows the water contact angle of SWPUA with different acrylate contents and the values are summarized in **Table 3.2**. The hydrophobic properties of SWPUA depend on the content of the internal emulsifier, polar group, and hydrophobic moieties. Generally, waterborne systems exhibit contact angles smaller than 90° because of hydrophilic groups. However, the contact angle of SWPUA-2 was 94.4° which can be attributed to the successful grafting of the acrylate unit (2-HEMA) with the WPU matrix to form a new hydrophobic semi-interpenetrating polymer network [6]. Furthermore, the

average molecular weight of all SWPUAs was determined by GPC analysis. It was observed that the weight-average molecular weight (M_w, $gmol^{-1}$) and number-average molecular weight (M_n, $gmol^{-1}$) of SWPUA-1, SWPUA-2, SWPUA-3, and SWPUA-4 were 173265 and 106876, 146783 and 91281, 151605 and 91996, and 150184 and 92194, respectively (**Table 3.2**). The polydispersity index (PDI) values were observed in the range of 1.607 - 1.647. The low PDI values correspond to the uniform polymeric chain, resulting in well-defined thermo-mechanical and self-healing properties [10-11]. Furthermore, the visible light transmittance values of SWPUA-1, SWPUA-2, SWPUA-3, and SWPUA-4 were 71%, 87%, 83%, and 77%, respectively, as shown in **Figure 3.3 (f)**. The high transparency can be attributed to the small particle size distribution and poor crystallinity of SWPUA films [12].

3.3.3. Thermal properties SWPUA films

The thermal properties of all films were investigated from the TGA and DSC analyses as shown in **Figure 3.4** and summarized in **Table 3.3**. Results showed that all the compositions exhibited good thermal stability. Generally, the main factors responsible for the thermal stabilities are the degree of polymerization i.e., the number of urethane linkages, the ratio of hard segment to soft segment, the number of aromatic moieties, molecular weight distribution, and the extent of physico-chemical cross-linking [13]. The TGA and DTG curves demonstrated that all SWPUAs undergo three-step thermal degradations and the corresponding temperatures are denoted as T_1, T_{MAX}, and T_2. A similar thermal degradation pattern of WPUA was reported by Qiu and co-workers [14]. The first step degradation (T_1) was observed in the range of 235.2 - 256.8 ℃.

Table 3.3. Thermal properties of SWPUAs.

Property	SWPUA-1	SWPUA-2	SWPUA-3	SWPUA-4
T_1 (℃)	251.6	249.7	235.2	250.3
T_{MAX} (℃)	327.7	326.9	329.3	328.4
T_2 (℃)	418.2	422.0	415.5	419.5
T_g (℃)	54.3	46.8	47.1	39.3

This step can be attributed to the degradation of weak dynamic disulfide bonds and the long aliphatic hydrocarbon chain of MG_{CO} [8]. Noticeably, a great extent of mass loss was found in the second step of thermal degradation (T_{MAX}) in the range of 328.4 - 330.3 °C because of the deterioration of relatively more thermostable moieties like carbamate group, ester linkages, and IPDI moieties.

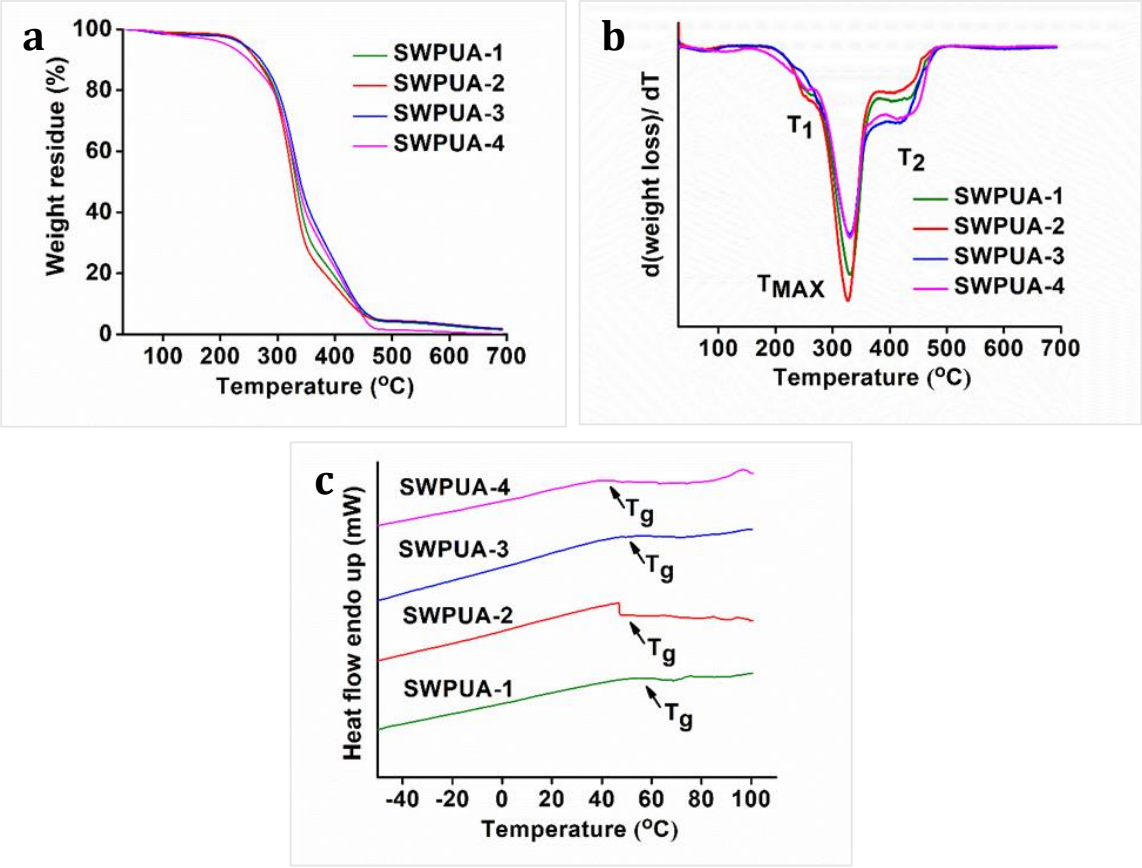

Figure 3.4. (a) TGA thermograms, (b) DTG curves, and (c) DSC curves of SWPUA films.

Again, the final step of degradation (T_2> 415 °C) corresponds to the most thermostable units including the aromatic ring of 2-APDS, carbon char, and ash formation process. GECA has a great effect on the thermal stability of all films. It contains two primary hydroxyl groups and two secondary hydroxyl groups which cause a high degree of chemical cross-linking, resulting in high thermal stability. Moreover, **Figure 3.4 (c)** shows the DSC curves of all SWPUAs. The glass transition temperatures (T_g) of SWPUA-1, SWPUA-2, SWPUA-3, and SWPUA-4 were 54.3 °C, 46.8 °C, 47.1 °C, and 39.3 °C, respectively.

3.3.4. Mechanical performances of SWPUA films

The mechanical properties of all SWPUAs were studied and the values are tabulated in **Table 3.4**. The stress-strain profiles of SWPUA are shown in **Figure 3.5 (a)**. It was observed that all films exhibited moderate tensile strength and average strain (%) at break. Here, the

moderate tensile strength of the SWPUA films can be accredited to high molar mass, multiple hydrogen bonds, rigidly structured benzene ring, and cycloaliphatic IPDI ring.

Table 3.4. Mechanical properties of SWPUA films.

Property	SWPUA-1	SWPUA-2	SWPUA-3	SWPUA-4
Tensile strength (MPa)	7.28±0.52	9.56±0.38	8.53±0.70	4.58±0.54
Strain (%)	524±2	145±2	217±4	484±3
Toughness (MJm^{-3})	34.43±0.80	12.65±0.58	15.12±0.53	19.52±0.71
Scratch hardness (kg)	2±0.02	2±0.02	2±0.01	2±0.02

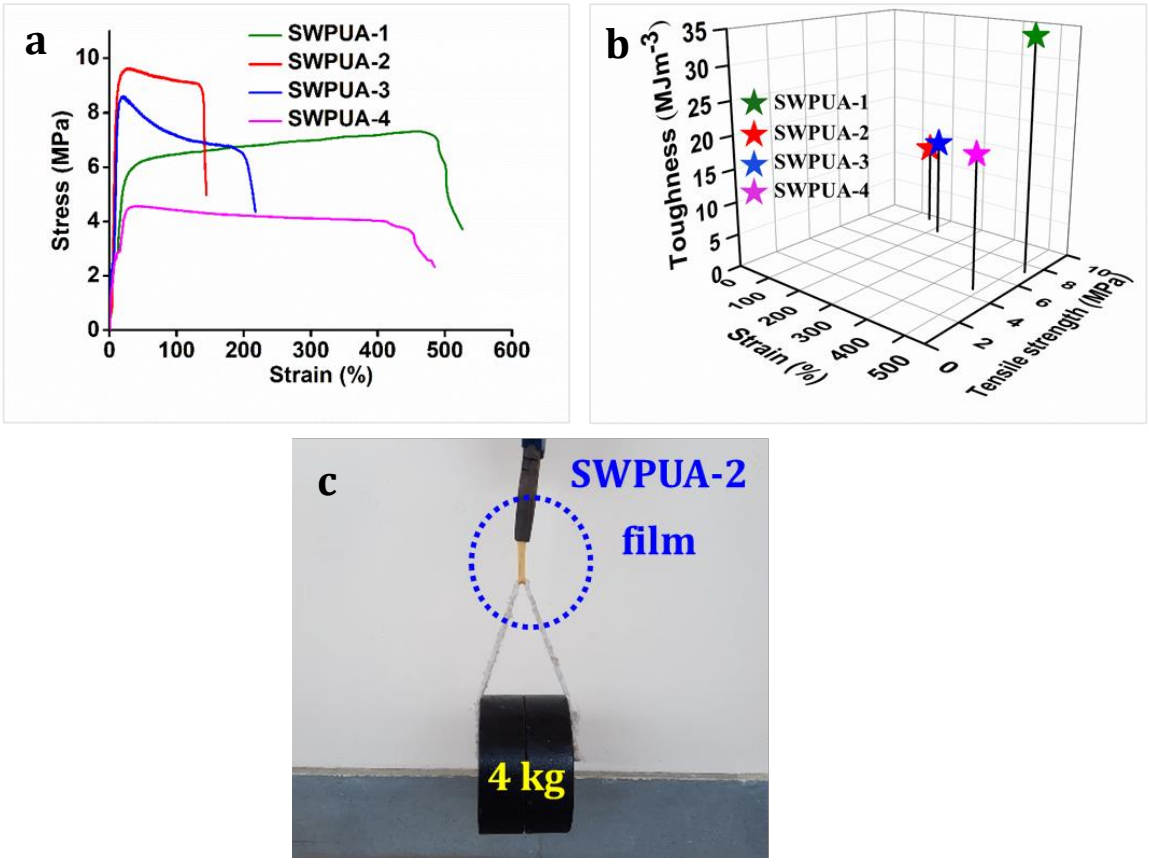

Figure 3.5. (a) Stress-strain profiles, (b) toughness of SWPUAs, and (c) showing a load of 4 kg lifted using an SWPUA-2 film.

The multiple hydrogen bonding develops physical cross-linking in the PU matrix. The MG_{CO} contains three hydroxyl groups (two primary and one secondary), while GECA contains

four hydroxyl groups (two primary and two secondary). So, crosslinking is sufficient to cause high mechanical strength. Additionally, the grafting of acrylate monomer via urethane bond formation and semi-interpenetrating network formation via free radical polymerization provide more increment in the final tensile strength [15]. The grafted polymer i.e., SWPUA-2 showed the highest tensile strength and very low strain (%) at break, as expected. The tensile strength and elongation of SWPUA-2 were 5.79±0.1 MPa and 121±1%, respectively. The high tensile strength and average stretchability caused the polymeric film to be mechanically tough. In this study, the toughness was measured by integrating the area under the stress-strain curve (**Figure 3.5 (b)**). As shown in **Figure 3.5 (c)**, it has been observed that a SWPUA-2 film could be used to lift a load of 4 kg which also supports its high toughness. Furthermore, scratch hardness of all SWPUAs was found to be good which can be attributed to the formation of semi-interpenetrating polymer and good tensile strength.

Table 3.5. Time (s) required for healing of SWPUA films under microwave radiation.

Power (W)	SWPUA-1	SWPUA-2	SWPUA-3	SWPUA-4
800	300 s	330 s	300 s	300 s
700	390 s	400 s	380 s	390 s
600	520 s	550 s	520 s	530 s

3.3.5. Self-healing and re-processability performances of SWPUA films

The healing efficiency of all SWPUAs was studied quantitatively by evaluating the change in the mechanical strength using UTM. All original samples were cut in the transverse direction with a length and thickness of 5 mm and 0.55 mm, respectively, and then put inside the microwave oven for the specified power and time until completely healed and the results were summarized in **Table 3.5**. To investigate the effect of acrylate moiety on the healing efficiency of the resultant polymer, various acrylates were incorporated into the WPU matrix. The plausible self-healing mechanism is shown in **Figure 3.6 (a)**. Again, **Figure 3.6 (c-f)** demonstrated the changes in the stress-strain curves of the original films and the healed films, and the results were tabulated in **Table 3.6**. It was observed that the tensile strength and the strain (%) at break of the pristine sample SWPUA-2 were 9.56±0.3 MPa. However, the value was changed to 5.30 ± 0.2 MPa after the first time of healing at 800 W for 330 s, which indicates an efficiency of 55.44% [16]. The healing process involves various steps such as segmental surface rearrangement, surface approach, wetting, diffusion, and

randomization [17]. Different polar groups present on the damaged surface absorbed the necessary energy from the microwave radiation which helped to oscillate their dipoles.

Table 3.6. Mechanical properties of the SWPUA films after healing at 800 W.

Samples	Healing Cycle	Tensile strength (MPa)	Healing efficiency (%)
SWPUA-1	1st	4.93±0.71	67.71
SWPUA-2	1st	5.30±0.29	55.44
SWPUA-3	1st	6.42±0.46	75.26
SWPUA-4	1st	3.78±0.28	82.53

This oscillation generates the rapid Brownian motion of the soft segment which leads to molecular chain diffusion below the melting temperature (T_m). In the present study, the healing process was intrinsically triggered by multiple hydrogen bonding and disulfide metathesis in the PU matrix. The metathesis can be considered to be a radical-mediated reaction in which homolytic cleavage of the disulfide bond occurs to create new sulfur-based radicals [18]. Finally, these radicals participate in the new disulfide bond formation (low activation energy, E_a of 20-50 $kJmol^{-1}$) assisted by microwave radiation to heal the fractured surfaces [19]. It has been observed that there is no significant change in the healing efficiency of the final polymer due to any acrylate group. So, it can be concluded that the healing ability is raised because of the presence of polar groups (especially, hydrogen bonds) and dynamic disulfide interchange reactions. The qualitative investigation of the healing ability of SWPUA-2 was carried out in an optical microscope. The big scratch on the sample almost disappears in about 330 s at a microwave power of 800 W, as shown in **Figure 3.6 (g)** and **(h)**. Additionally, more experiments have been performed to demonstrate the self-healing ability of SWPUA-2 visually. A film was cut into three pieces and two of them were stained with malachite green and methyl red. Then, the pieces were connected and healed as shown in **Figure 3.6 (b)**. The healed sample can lift a weight of 500 g and can be stretched to large deformation without any damage as shown in **Figure 3.6 (i)** and **(j)**. It is pertinent to mention that the dynamic disulfide bonds and hydrogen bonds induce good re-processability in SWPUA films [20]. The test was performed by cutting the sample into small pieces and hot-pressed in a compression molding machine at 60 °C under the pressure of 60-80 $kg\ cm^{-2}$

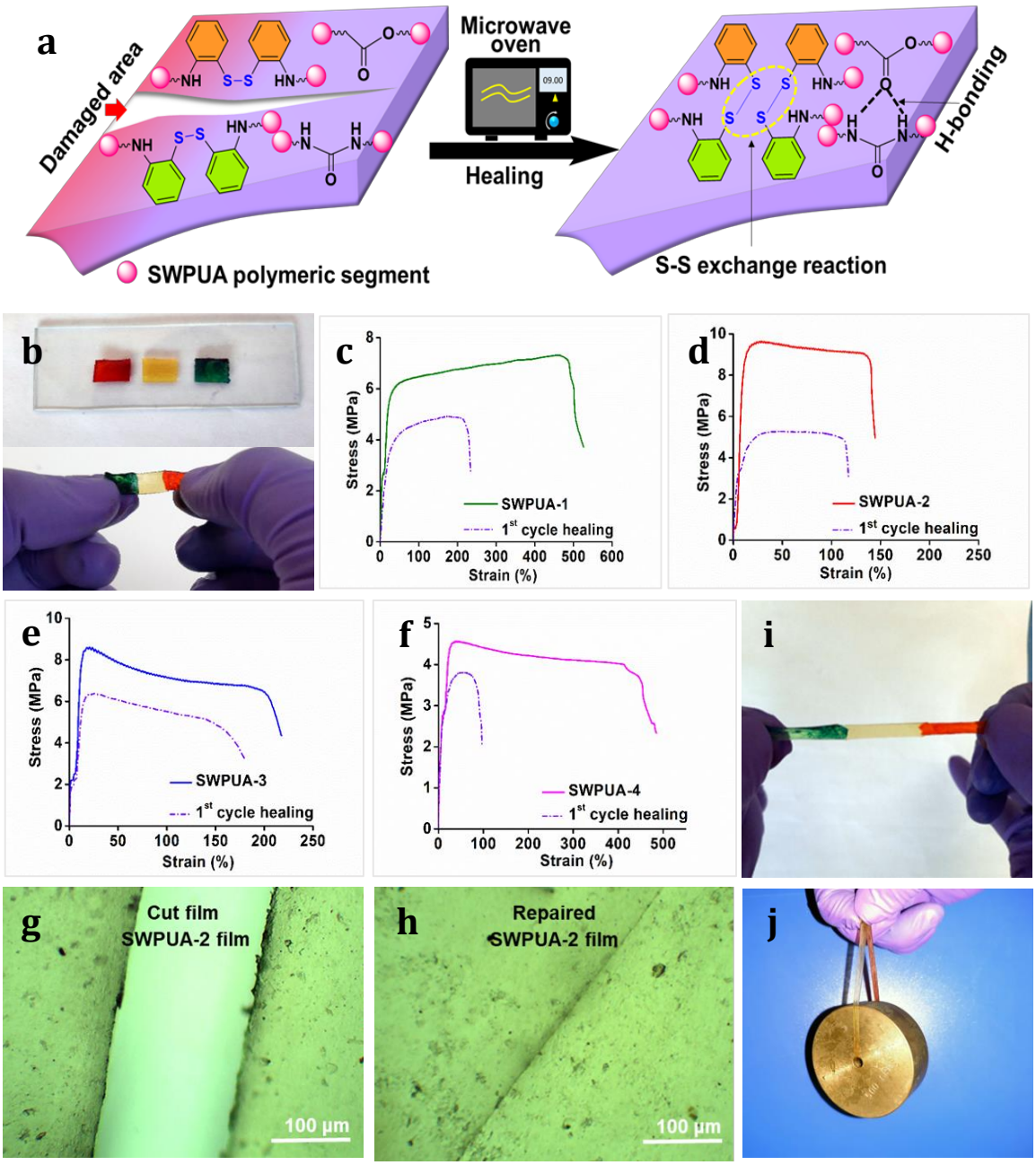

Figure 3.6. (a) Possible healing mechanism, (b) three pieces of the cut film before healing and joined the film after healing at 800 W for 330 s, (c-f) stress-strain profile of SWPUA film after 1st cycle of healing at 800 W for 330 s, (g-h) optical microscopic images of crack and healing films (SWPUA-2), and (i-j) stretching and weight-lifting test after healing of SWPUA-2.

for 30 min without using any solvent or catalyst (**Figure 3.7 (a)** and **(b)**). The recovery efficiencies for the mechanical properties are shown in **Figure 3.7 (d)** and summarized in **Table 3.7**. After repeated reprocessing, all films exhibit acceptable tensile strength. The first cycle reprocessing efficiency (tensile strength) of SWPUA films (R1 SWPUAs) varies from 77.51% to 92.57%. Furthermore, thermal stability was also marginally improved after reprocessing as shown in **Figure 3.7 (e)**. Thus, it can be concluded that the excellent self-healing ability and re-processable capability of the newly synthesized SWPUA film would

prolong its service life, resulting in sustainability via reducing environmental pollution and raw materials waste [21].

Table 3.7. Mechanical data of the SWPUA films after reprocessing.

Samples	Tensile strength (MPa)	Recycle efficiency (%)	Strain (%) at break	Recycle efficiency (%)
R1 SWPUA-1	6.02±0.32	82.69	360±5	68.70
R1 SWPUA-2	8.85±0.28	92.57	126±2	86.89
R1 SWPUA-3	7.83±0.25	91.79	189±2	87.09
R1 SWPUA-4	3.55±0.41	77.51	417±2	86.15

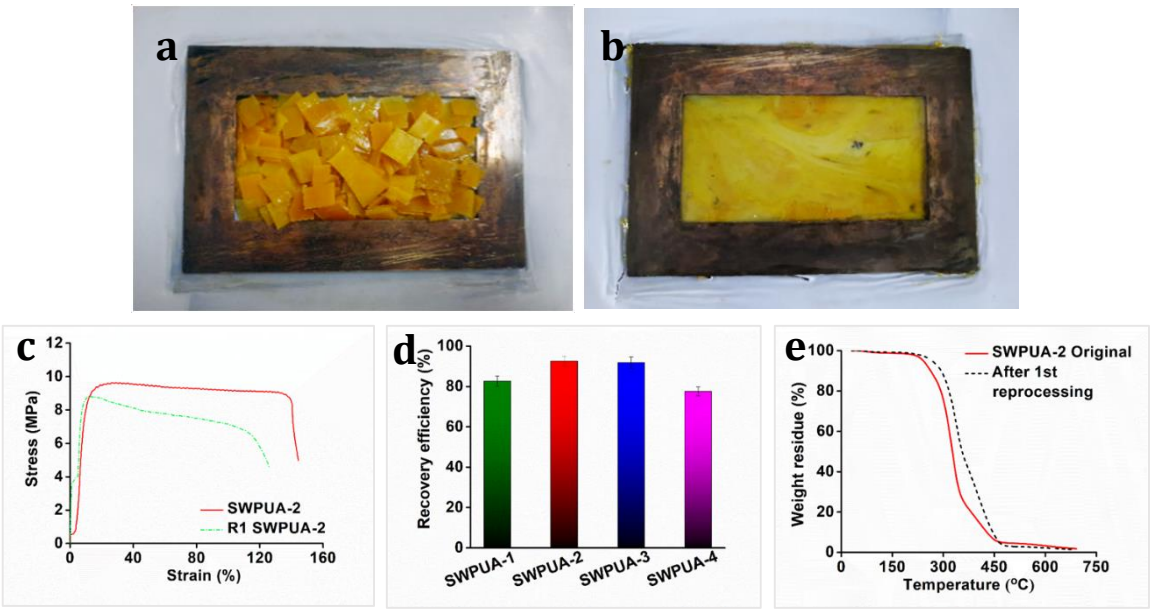

Figure 3.7. (a-b) Digital images of reprocessed SWPUA-2 film at 60 °C with a pressure of 60-80 kg cm-2 in 30 min, (c) stress-strain profiles of SWPUA-2 after 1st cycle (R1 SWPUA-2) of reprocessing, (d) tensile strength recovery (%) of SWPUA film after 1st cycle of reprocessing, and (e) TGA thermograms of pristine and reprocessed SWPUA-2 film.

3.3.6. Biocompatibility evaluation

The proliferation of L929 cells on three different concentrations of SWPUA-2 material was analyzed by MTT assay [22]. **Figure 3.8** shows that all the concentrations indicate comparable cell proliferation to that of the tissue culture microliter plate after 24 h and 72 h of incubation. The percentage of cell viability of 10% SWPUA-2, 20% SWPUA-2, and 30%

SWPUA-2 on 24 h were 88.14%, 81.52%, and 75.23%, respectively. The 72 h showed 79.5%, 74.07%, and 70.39% cell viability, respectively.

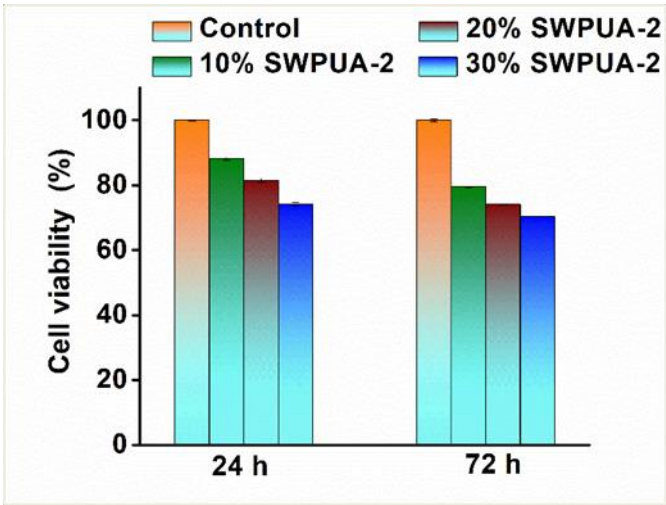

Figure 3.8. Cell viability studies of L929 cells treated with different concentrations of SWPUA-2 solution (10%, 20%, 30%) after 24 h and 72 h.

As a result, the in vitro cytotoxicity assays revealed that all doses of SWPUA-2 (10%, 20%, and 30%) were capable of sustaining the development of cells and did not demonstrate any cytotoxicity after three days of incubation. The results are shown as a percentage of cell proliferation at various periods in various treatment groups.

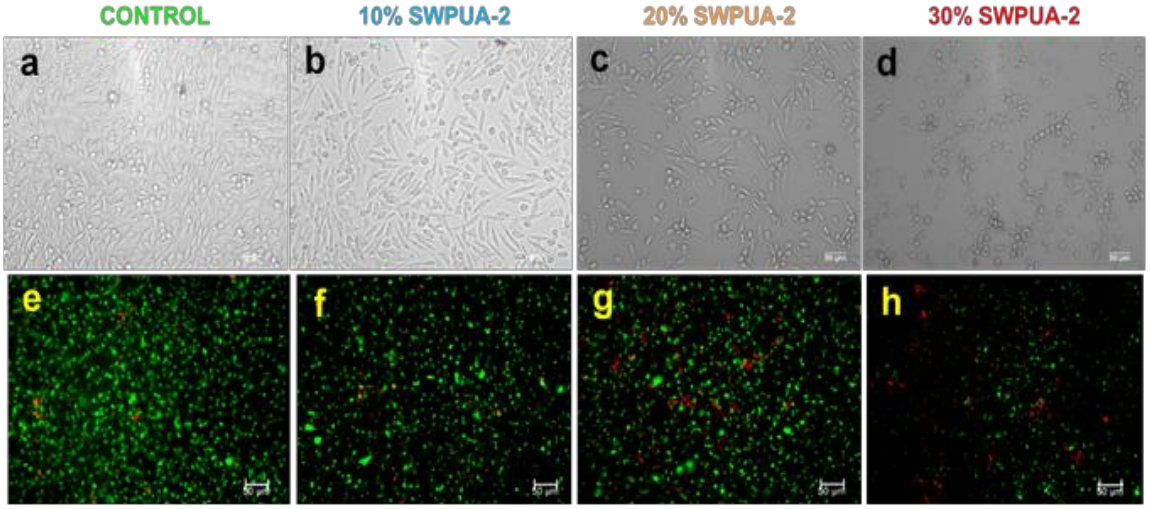

Figure 3.9. (a-d) Bright-field micrographs, (e-h) Live/dead staining of L929 cells treated with control and various percentages of SWPUA-2 solution (10%, 20%, and 30%) after 3 days of incubation (scale bar: 50 μm).

Moreover, dead cells stained with EtBr fluoresced red, whereas living cells stained with calcein AM fluoresced green. In **Figure 3.9**, cells treated with 30% SWPUA-2 solution showed a rounder shape compared to the normal fibroblast morphology due to the higher hydrophobicity of the SWPUA-2 material. However, in 10% and 20% SWPUA-2, more cells with fibroblast morphology can be seen. These two compositions showed fewer dead cells after 3 days of cell culture. As increasing the concentration of SWPUA-2 the number of cells

is decreasing. *In vitro*, the biocompatibility of the various concentrations of SWPUA 2 enables cellular adhesion and proliferation of L929 cells, according to investigations on cellular viability and proliferation [23].

3.3.7. UV-curable SWPUA/GelMA/gelatin-based ink for biomedical scaffold preparation

The ink composition and optimized processing parameters are mentioned in **Table 3.8** and printed as the model articles like slice-cuboid and sliced-disc (**Figure 3.10 (a)**). Scaffolds were kept under UV radiation at a range of 365 - 410 nm after printing, with some extent of cross-linking. Then printed scaffolds were kept in a hot air oven for 48 h at 50 ℃ for drying. As shown in **Figure 3.10 (b)** and **(c)**, the cuboid and disc scaffolds are shown to be dimensionally stable; however, as layer height grew, the results showed decreased porosity.

Table 3.8. Optimized ink composition and machine parameters of the 3D printing.

Parameter/ composition	Cuboid	Disc
Dimension	2.5 cm × 2.5 cm × 2 cm (Length × width × height)	1.5 cm (ID), 2.9 cm (OD), 0.5 cm (Thickness)
Solution A	GelMA 20% (wt/v)/ SWPUA-2, (1:1, v/v)	GelMA 20% (wt/v)/ SWPUA-2, (1:1, v/v)
Solution B	Gelatin 20% (wt/v)	Gelatin 20% (wt/v)
Ink composition	Solution A/ Solution B (0.6:0.4, v/v)	Solution A/ Solution B (0.6:0.4, v/v), added a few drops of bromophenol blue indicator
Layer height	0.35 mm	0.25 mm
Shell Thickness	0.40 mm	0.30 mm
Fill density	20%	15%
Flow rate	20%	20%
Printing speed	6.0 mm/s	8.0 mm/s

The optimized composition of the ink demonstrated good printability showing enough scaffold heights (around 5 mm) with an optimized concentration of GelMA and gelatin in the SWPUA-2. The SWPUA-2 solution showed adequate biocompatibility against L929 fibroblast cells. The other two materials, namely, photo-cross-linkable GelMA, and gelatin, are well-known biocompatible materials that have been studied a lot in biomedical applications for scaffolds in the tissue engineering that promote cell growth, adhesion, and

function [24]. Increased layers height led to the accumulation of extruded materials at cross-sectional points, which showed that covering the pores, causing reduced porosity.

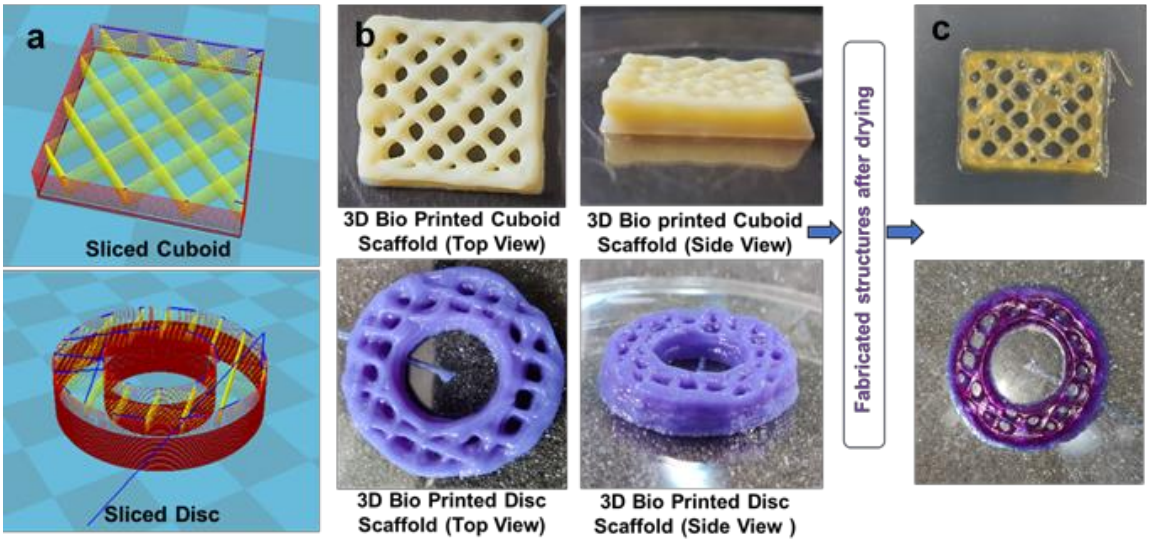

Figure 3.10. (a) 3D slicing model of cuboid and disc and (b-c) 3D bio-printed cuboid and disc scaffolds before and after drying.

The printed scaffold's height and material spill problem can be addressed by adding more gelatin percentage or other natural polymers, such as alginate (ionic cross-linked) and fillers, by controlling process parameters such as bed temperature, ink, and environment temperature [24]. Dried scaffolds were found to be dimensionally stable at room temperature. The GelMA/gelatin/SWPUA-2-based ink was printable, and its dried scaffolds showed dimensionally stable. To improve their properties like mechanical strength, reduced degradability, porosity, and biocompatibility, many approaches can be used, such as the incorporation of nanomaterials (nano clay and CNTs), making blends, and use of biocompatible cross-linkers for gelatin and SWPUA-2 [25]. The printed scaffolds can potentially treat articular cartilage defects by incorporating mesenchymal stem cells (MSCs) and can be used in wound healing and bone regeneration [26-27].

3.3.8 Biodegradation of SWPUA films

The partial biodegradability of SWPUA films was established by plotting weight loss percentage against time following a soil burial test. The weight loss of buried SWPUA films was determined after 120 days. **Figure 3.11 (a)** shows that the weight loss percentage of the polymeric film increases with time. Thus, the SWPUA films prepared in this study are biodegradable in the soil environment. Moreover, SEM images and their 3D surface images (**Figure 3.11 (b-e)**) demonstrated the bacterial growth on the SWPUA films. The surface of the biodegraded film is craggier than the non-degraded film. The four steps that are essential for biodegradations include permeation of water molecules, hydrolysis of ester groups,

solubilization of these groups, and transformation into water, CO_2, and humus by enzymes and bacteria.

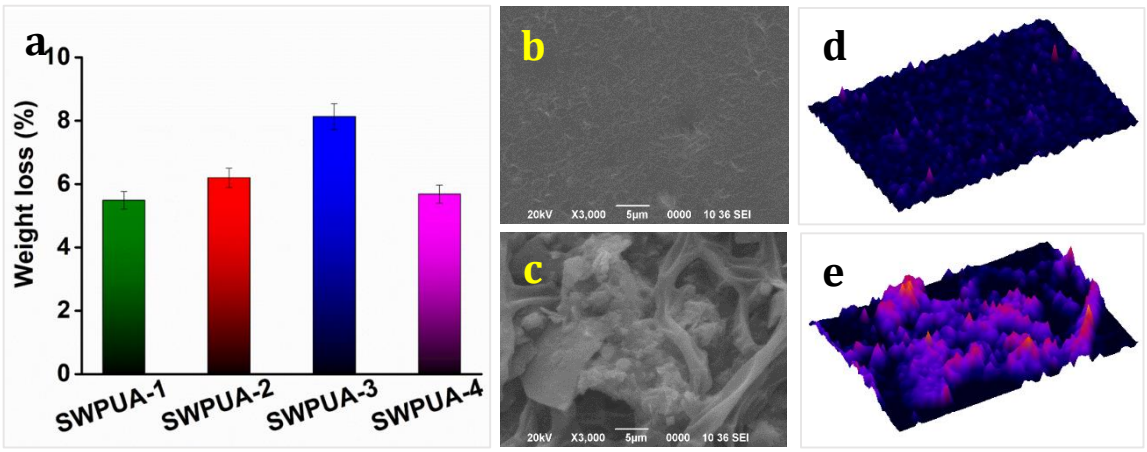

Figure 3.11. (a) Weight loss (%) after 120 days of the soil burial test, (b-c) SEM images of controlled (un-degraded) and degraded films of SWPUA-2, respectively, and (d-e) 3D surface plots of the SEM images obtained from ImageJ software.

Some bacteria such as *P. aeruginosa* and *B. subtilis*, can easily attack the hydrolyzable groups (e.g., ester groups of PCL, MG_{CO}, and GECA) of the PU matrix and help in the deterioration process [28-29].

3.4 Conclusion

In conclusion, based on the triple synergistic effect of 'dynamic hard domain', 'multiple hierarchical hydrogen bonding', and 'semi-interpenetrating network (IPN) formation' to synthesize a series of biobased SWPUA dispersions to address the dilemma that existed between high mechanical strength and good healing efficiency in a single WPU elastomer under solvent-free and surfactant-free conditions. The synthesis process merges the two polymerization mechanisms i.e., step-growth and free radical chain-growth polymerizations. At the initial stage, acrylate monomers act as the diluent to reduce the viscosity of the polymerized polyurethane medium and at the final stage they are polymerized via seeded mini-emulsion free radical polymerization by KPS. 2-APDS was introduced into the WPU matrix as the hard domain with dynamic S-S linkages to achieve optimum healing efficiency and mechanical properties. Impressively, the resulting films exhibited good mechanical robustness and thermal stability along with good self-healing ability in the presence of microwave radiation. The reversible and dynamic S-S bond and multiple hierarchical hydrogen bonds are responsible for good healing ability. Concurrently, the rigid benzene rings and short-chain acrylate moieties enhance the ultimate tensile strength. A load of 4 kg can be lifted vertically and successfully by an SWPUA film (0.377g) which is 10,610 times heavier than its weight. Additionally, all films are biodegradable and re-processable under

mild conditions. Most importantly, the MTT assay and live/dead assay of L929 cells on SWPUA dispersion established the biocompatibility nature. Furthermore, the SWPUA/GelMA/gelatin ink can be used for developing sliced cuboid and disc scaffolds. These scaffolds have the potential for the treatment of articular cartilage defects by incorporating MSCs, in wound healing, and bone regeneration.

References

[1] Zhu, X., Han, K., Li, C., Wang, J., Yuan, J., Pan, Z. and Pan, M. Tough, Photoluminescent, self-healing waterborne polyurethane elastomers resulting from synergistic action of multiple dynamic bonds. *ACS Applied Materials & Interfaces*, 15(15):19414-19426, 2023.

[2] An, Z. W., Xue, R., Ye, K., Zhao, H., Liu, Y., Li, P., Chen, Z. M., Huang, C. X. and Hu, G. H. Recent advances in self-healing polyurethane based on dynamic covalent bonds combined with other self-healing methods. *Nanoscale*, 15(14):6505-6520, 2023.

[3] Kim, S. M., Jeon, H., Shin, S. H., Park, S. A., Jegal, J., Hwang, S. Y., Oh, D. X. and Park, J. Superior toughness and fast self-healing at room temperature engineered by transparent elastomers. *Advanced Materials*, 30(1):1705145, 2018.

[4] Wang, D., Xu, J., Chen, J., Hu, P., Wang, Y., Jiang, W. and Fu, J. Transparent, mechanically strong, extremely tough, self-recoverable, healable supramolecular elastomers facilely fabricated via dynamic hard domains design for multifunctional applications. *Advanced Functional Materials*, 30(3):1907109, 2020.

[5] Zhang, L., Liu, Z., Wu, X., Guan, Q., Chen, S., Sun, L., Guo, Y., Wang, S., Song, J., Jeffries, E. M. and He, C. A highly efficient self-healing elastomer with unprecedented mechanical properties. *Advanced Materials*, 31(23):1901402, 2019.

[6] Van Den Bulcke, A. I., Bogdanov, B., De Rooze, N., Schacht, E. H., Cornelissen, M. and Berghmans, H. Structural and rheological properties of methacrylamide modified gelatin hydrogels. *Biomacromolecules*, 1(1):31-38, 2000.

[7] Jiang, T., Yang, T., Bao, Q., Sun, W., Yang, M. and Mao, C. Construction of tissue-customized hydrogels from cross-linkable materials for effective tissue regeneration. *Journal of Materials Chemistry B*, 10(25):4741-4758, 2022.

[8] Chen, R., Zhang, C. and Kessler, M. R. Anionic waterborne polyurethane dispersion from a bio-based ionic segment. *RSC Aadvances*, 4(67):35476-35483, 2014.

[9] Lopez, A., Degrandi-Contraires, E., Canetta, E., Creton, C., Keddie, J. L. and Asua, J. M. Waterborne Polyurethane− Acrylic hybrid nanoparticles by Miniemulsion polymerization: applications in pressure-sensitive adhesives. *Langmuir*, 27(7):3878-3888, 2011.

[10] Li, M., Daniels, E. S., Dimonie, V., Sudol, E. D. and El-Aasser, M. S. Preparation of polyurethane/acrylic hybrid nanoparticles via a miniemulsion polymerization process. *Macromolecules*, 38(10):4183-4192, 2005.

[11] Rane, S. S. and Choi, P. Polydispersity index: how accurately does it measure the breadth of the molecular weight distribution? *Chemistry of materials*, 17(4):926-926, 2005.

[12] Chen, L., Qian, J.Y., Zhu, D. D., Yang, S., Lin, J., He, M. Y., Zhang, Z. H. and Chen, Q. Mesoporous zeolitic imidazolate framework-67 nanocrystals on siliceous mesocellular foams for capturing radioactive iodine. *ACS Applied Nano Materials*, 3(6):5390-5398, 2020.

[13] Dai, Z., Jiang, P., Lou, W., Zhang, P., Bao, Y., Gao, X., Xia, J. and Haryono, A. Preparation of degradable vegetable oil-based waterborne polyurethane with tunable mechanical and thermal properties. *European Polymer Journal*, 139:109994, 2020.

[14] Xu, H., Qiu, F., Wang, Y., Wu, W., Yang, D. and Guo, Q. UV-curable waterborne polyurethane-acrylate: preparation, characterization and properties. *Progress in Organic Coatings*, 73(1):47-53, 2012.

[15] Mehravar, S., Ballard, N., Agirre, A., Tomovska, R. and Asua, J. M. Role of grafting on particle and film morphology and film properties of zero VOC polyurethane/poly (meth) acrylate hybrid dispersions. *Macromolecular Materials and Engineering*, 304(2):1800532, 2019.

[16] Sun, F., Liu, L., Xu, J. and Fu, J. Smart healable polyurethanes: Sustainable problem solvers based on constitutional dynamic chemistry. *Materials Chemistry Frontiers*, 7:3494-3523, 2023.

[17] Burattini, S., Greenland, B. W., Chappell, D., Colquhoun, H. M. and Hayes, W. Healable polymeric materials: A tutorial review. *Chemical Society Reviews*, 39(6):1973-1985, 2010.

[18] Nevejans, S., Ballard, N., Miranda, J. I., Reck, B. and Asua, J. M. The underlying mechanisms for self-healing of poly(disulfide)s. *Physical Chemistry Chemical Physics*, 18(39):27577-27583, 2016.

[19] Zhang, M., Zhao, F. and Luo, Y. Self-healing mechanism of microcracks on waterborne polyurethane with tunable disulfide bond contents. *ACS omega*, 4(1):1703-1714, 2019.

[20] Xue, R., Zhao, H., An, Z. W., Wu, W., Jiang, Y., Li, P., Huang, C. X., Shi, D., Li, R. K., Hu, G. H. and Wang, S. F. Self-healable, solvent response cellulose nanocrystal/waterborne polyurethane nanocomposites with encryption capability. *ACS Nano*, 17(6):5653-5662, 2023.

[21] Xu, X., Wu, J., Li, M., Wang, S., Feng, H., Wang, B., Hu, K., Zhang, C., Zhu, J. and Ma, S. Synergistic catalytic effect of triple dynamic bonds for fast-reprocessing and high-performance cross-linked polymers. *Polymer Chemistry*, 14(4):523-532, 2023.

[22] Xie, J., Tian, S., Zhang, H., Feng, C., Han, Y., Dai, H. and Yan, L. A Novel NQO1 Enzyme-responsive polyurethane nanocarrier for redox-triggered intracellular drug release. *Biomacromolecules*, 24(5):2225-2236, 2023.

[23] Zenoozi, S., Sadeghi, G. M. M. and Rafiee, M. Synthesis and characterization of biocompatible semi-interpenetrating polymer networks based on polyurethane and cross-linked poly (acrylic acid). *European Polymer Journal*, 140:109974, 2020.

[24] Wang, Y. J., Jeng, U. S. and Hsu, S. H. Biodegradable water-based polyurethane shape memory elastomers for bone tissue engineering. *ACS Biomaterials Science & Engineering*, 4(4):1397-1406, 2018.

[25] Gao, Q., Niu, X., Shao, L., Zhou, L., Lin, Z., Sun, A., Fu, J., Chen, Z., Hu, J., Liu, Y. and He, Y. 3D printing of complex GelMA-based scaffolds with nanoclay. *Biofabrication*, 11(3):035006, 2019.

[26] Yu, C., Schimelman, J., Wang, P., Miller, K. L., Ma, X., You, S., Guan, J., Sun, B., Zhu, W. and Chen, S. Photopolymerizable biomaterials and light-based 3D printing strategies for biomedical applications. *Chemical reviews*, 120(19):10695-10743, 2020.

[27] Ravi, S., Chokkakula, L. P., Giri, P. S., Korra, G., Dey, S. R. and Rath, S. N. 3D bioprintable hypoxia-mimicking peg-based nano bioink for cartilage tissue engineering. *ACS Applied Materials & Interfaces*, 15(16):19921-19936, 2023.

[28] Wang, M., Liu, H. Y., Ke, N. W., Wu, G., Chen, S. C. and Wang, Y. Z. Toward regulating biodegradation in stages of polyurethane copolymers with bicontinuous microphase separation. *Journal of Materials Chemistry B*, *11*(14):3164-3175, 2023.

[29] Liu, X., Wang, S., Liu, Y., Yao, Y., Zhu, X., Hu, Y., Wan, T. and Cheng, B. Synthesis of poly (ether carbonate)-based polyurethane for biodegradable–recyclable pressure sensors. *ACS Sustainable Chemistry & Engineering*, 11(10):4258-4268, 2023.